Contrast-to-Noise Ratios of Diffusion Anisotropy Indices

Peter B. Kingsley[1,2]* and W. Gordon Monahan[1,2]

The degree of diffusion anisotropy in different brain regions is usually measured by a diffusion anisotropy index (DAI) such as relative anisotropy (RA) and fractional anisotropy (FA). FA has been reported to have a higher contrast-to-noise ratio (CNR) than RA. The present work compares the CNRs of seven DAIs in theoretical propagation-of-error calculations, in simulations, and in human brain measurements over small and large anisotropy differences. In simulations all seven CNRs were similar for small anisotropy differences. Small differences among the DAIs appeared at higher anisotropy levels and lower signal-to-noise ratios with certain tensor orientations. The DAIs fell into three groups based on algebraic relationships and small CNR differences. The group with RA and FA had the best CNR. Human brain regions with small anisotropy differences had similar CNR for all seven DAIs, and the scatter in the data was greater than any expected differences. With large anisotropy differences, a small advantage appeared for RA over FA in some simulations and for FA over RA in other simulations. The CNR between brain regions with very different anisotropies was different for each DAI. The apparent reported advantage of FA over RA is explained by biologic heterogeneity and by noise-induced bias in the DAI values and their standard deviations. Magn Reson Med 53:911–918, 2005. © 2005 Wiley-Liss, Inc.

Key words: anisotropy; diffusion tensor; fractional anisotropy; MRI; noise

Diffusion tensor imaging (DTI) has been useful for measuring the degree of diffusion anisotropy in different brain regions (1–10) and in diseases that involve the brain. The degree of anisotropy is usually expressed by a number called a diffusion anisotropy index (DAI), which can be calculated from the diffusion eigenvalues λ_1, λ_2, and λ_3 (Table 1) (1–5,8,11) or from the diffusion tensor elements (5–9,12). The first three definitions of rotationally invariant DAIs that do not require eigenvalue sorting were the relative anisotropy (RA), the fractional anisotropy (FA), and the volume ratio (VR) (13). In order to make each DAI range from 0 for isotropic diffusion to 1 for completely anisotropic (unidirectional) diffusion, the volume fraction (VF = 1 − VR) (2) and $A_\sigma = \mathrm{RA}/2^{1/2}$ (12) were defined. These modified DAIs will be used in the present work, but A_σ will be referred to as "scaled RA," sRA, because the name "relative anisotropy" is better known. Other DAIs were suggested later, including three "ultimate anisotropy" indices ($\mathrm{UA_{surf}}$, $\mathrm{UA_{vol}}$, and $\mathrm{UA_{vol,\ surf}}$) (7) and the γ-variate anisotropy index (GV), which is computed from sRA (4).

The main application of DAIs is to determine whether two tissues have the same degree of anisotropy. The tissues may differ in age, location, or disease state. In these cases the important parameter for DAI comparisons is the contrast-to-noise ratio (CNR), which is very similar to Student's *t* statistic. Other parameters such as contrast alone (4,7), noise alone, and signal-to-noise ratio (SNR) (3,8) do not, by themselves, indicate anything about the ability to differentiate tissues with different anisotropy levels.

The three original DAIs (RA, FA, and VR) have been compared with respect to CNR in human brain between different tissues (2) and in simulations comparing anisotropic tissues and isotropic diffusion (10), as well as with respect to SNR in simulations (3,8) and in human brain (8). However, there do not appear to have been any systematic comparisons with the other four DAIs, with analytic propagation-of-error calculations, or with CNR with a small difference in sRA in simulations. This latter definition is important for optimizing the detection of small differences between different brain regions or different groups, for example a diseased brain compared to a normal brain. Furthermore, despite a claim that "FA exhibits better noise immunity characteristics" than sRA (8), no consistent advantage of any DAI over any other DAI for statistical comparison of anisotropy in homogeneous regions with uniform anisotropy has ever been demonstrated.

The purpose of this work is to compare the CNR of all seven DAIs in Table 1 for both small and large anisotropy differences. These comparisons include analytic propagation-of-error calculations, Monte Carlo simulations, and experimental data.

THEORY

The different DAIs can be divided into three groups based on algebraic relationships. Fractional anisotropy (9), $\mathrm{UA_{surf}}$, GV, and sRA can be expressed in terms of each other,

$$\mathrm{FA}^2 = 3\mathrm{sRA}^2/(2\mathrm{sRA}^2 + 1) = 3\mathrm{RA}^2/(2\mathrm{RA}^2 + 2) \quad [1]$$

$$\mathrm{UA_{surf}} = 1 - (1 - \mathrm{sRA}^2)^{1/2} \quad [2]$$

$$\mathrm{GV} = [519.14 - 259.57e^{-8\mathrm{sRA}} \times (64\mathrm{sRA}^2 + 16\mathrm{sRA} + 2)]/512 \quad [3]$$

$$\mathrm{sRA}^2 = \mathrm{FA}^2/(3 - 2\mathrm{FA}^2) = 1 - (1 - \mathrm{UA_{surf}})^2, \quad [4]$$

$\mathrm{UA_{vol}}$ and VF can be expressed in terms of each other,

$$\mathrm{VF} = 1 - (1 - \mathrm{UA_{vol}})^3 \quad [5]$$

[1]Department of Radiology, North Shore University Hospital, Manhasset, New York, USA.

[2]Department of Radiology, New York University School of Medicine, New York, New York, USA.

Grant sponsor: Center for Advanced Magnetic Resonance Technology at Stanford; Grant number: P41RR009784.

*Correspondence to: Peter B. Kingsley, Department of Radiology/MRI, North Shore University Hospital, 300 Community Drive, Manhasset, NY 11030, USA. E-mail: pkingsle@nshs.edu

Received 4 August 2004; revised 19 November 2004; accepted 20 November 2004.

DOI 10.1002/mrm.20433
Published online in Wiley InterScience (www.interscience.wiley.com).

Table 1
Summary of DAI Formulas That Range from Zero (Isotropic) to One (Anisotropic)

Diffusion anisotropy index	Formula[a]
Scaled relative anisotropy (sRA)	$\{[(\lambda_1-D_{av})^2+(\lambda_2-D_{av})^2+(\lambda_3-D_{av})^2]/6\}^{1/2}/D_{av}$
Fractional anisotropy (FA)	$\{3[(\lambda_1-D_{av})^2+(\lambda_2-D_{av})^2+(\lambda_3-D_{av})^2]/[2(\lambda_1{}^2+\lambda_2{}^2+\lambda_3{}^2)]\}^{1/2}$
Volume fraction (VF)	$1-\lambda_1\lambda_2\lambda_3/D_{av}{}^3$
Gamma variate (GV)[b]	$[ae^{-bsRA}(b^2sRA^2+2bsRA+2)-2a]/b^3$, $a=-259.57$, $b=8$
UA_{surf}	$1-[(\lambda_1\lambda_2+\lambda_2\lambda_3+\lambda_3\lambda_1)/3]^{1/2}/D_{av}$
UA_{vol}	$1-(\lambda_1\lambda_2\lambda_3)^{1/3}/D_{av}$
$UA_{vol,surf}$	$1-(\lambda_1\lambda_2\lambda_3)^{1/3}/[(\lambda_1\lambda_2+\lambda_2\lambda_3+\lambda_3\lambda_1)/3]^{1/2}$

[a] $D_{av}=(\lambda_1+\lambda_2+\lambda_3)/3$.
[b] The b in the γ variate formula is not the diffusion sensitivity factor b. The γ-variate constants a and b can be selected freely and have been set to the values suggested in Ref. (4).

$$UA_{vol}=1-(1-VF)^{1/3}, \quad [6]$$

and $UA_{vol,\,surf}$ can be expressed in terms of sRA and VF:

$$UA_{vol,surf}=1-(1-VF)^{1/3}/(1-sRA^2)^{1/2}. \quad [7]$$

Equations [1–5] lead to the following relationships for the derivatives with respect to sRA or UA_{vol}: dFA/dsRA (8), dGV/dsRA (4), dUA_{surf}/dsRA, and dVF/dUA_{vol}.

$$dFA/dsRA=(FA/sRA)^3/3 \quad [8]$$

$$dGV/dsRA=259.57\,sRA^2e^{-8sRA} \quad [9]$$

$$dUA_{surf}/dsRA=sRA/(1-sRA^2)^{1/2} \quad [10]$$

$$dVF/dUA_{vol}=3(1-UA_{vol})^2 \quad [11]$$

DAIs are most commonly compared as a function of an anisotropy index defined for cylindrical symmetry (7,12), where two eigenvalues are equal (with a value equal to $D2$) and the third eigenvalue may be different (with a value equal to $D1$),

$$A=(D1-D2)/(D1+2D2)=(D1/D_{av}-1)/2, \quad [12]$$

where D_{av} is defined in Table 1. A ranges from -0.5 for completely anisotropic oblate diffusion ($D1=0$) through 0 for isotropic diffusion to 1 for completely anisotropic prolate diffusion ($D2=0$). The seven DAIs are plotted as a function of A in Fig. 1a, and their derivatives with respect to A are plotted in Fig. 1b. Since sRA = $|A|$ (Fig. 1), Fig. 1b also shows the derivatives with respect to sRA.

For comparisons among the DAIs, CNR is the statistically relevant parameter. Contrast is the difference between two DAI values, and the noise is the square root of the sum of the variances in the two individual measurements. In order to compare CNR over different anisotropy intervals, the CNR can be divided by the difference in some reference anisotropy index. A logical choice for such a reference index in simulations is A, since A = sRA for a prolate diffusion ellipsoid and because A and sRA are commonly used as a scale for comparing DAIs (2,4,7,8). Furthermore, for a fixed value of D_{av}, a plot of sRA as a function of the largest eigenvalue is linear both for cylindrical symmetry (Eq. [12]) and when $\lambda_1-\lambda_2=\lambda_2-\lambda_3$ (3). The resulting CNR formula is

$$CNR_2=[(DAI_2-DAI_1)/(A_2-A_1)]/(\sigma_1^2+\sigma_2^2)^{1/2}, \quad [13]$$

where DAI_1 and DAI_2 are the expectation values (averages) of the DAI calculated at each A value. The factor (A_2-A_1)

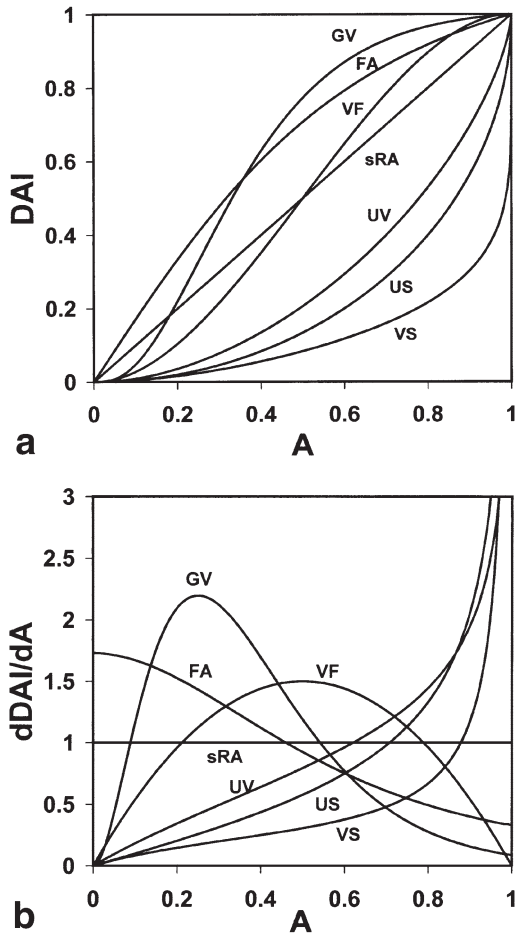

FIG. 1. Comparison of the seven DAIs as a function of A for a cylindrically symmetric prolate diffusion ellipsoid. **a**: DAI values. **b**: Derivatives with respect to A, which are also the derivatives with respect to sRA. UV, UA_{vol}; US, UA_{surf}; VS, $UA_{vol,\,surf}$.

in the denominator is simply a scale factor that allows comparison of CNR over different anisotropy intervals. It can be ignored when two DAIs are being compared over the same anisotropy interval. In the limit of an infinitesimal change in A, the relative CNR at a single A value becomes

$$\mathrm{CNR}_1 = (d\mathrm{DAI}/dA)/\sigma_A. \quad [14]$$

In biologic samples the measured DAI variance contains contributions from biologic heterogeneity as well as from noise. This additional factor can be emphasized by calling the measured CNR the CSR, for "contrast-to-scatter ratio" or "contrast-to-standard-deviation ratio." Furthermore, the true eigenvalues are not known and cylindrical symmetry may not be present. The $A_2 - A_1$ term can be omitted from Eq. [13] (2,8,10), or it can be replaced with $\mathrm{sRA}_2 - \mathrm{sRA}_1$:

$$\mathrm{CSR} = [(\mathrm{DAI}_2 - \mathrm{DAI}_1)/(\mathrm{sRA}_2 - \mathrm{sRA}_1)]/(\sigma_1^2 + \sigma_2^2)^{1/2}. \quad [15]$$

As in Eq. [13], the scale factor $(\mathrm{sRA}_2 - \mathrm{sRA}_1)$ in the denominator can be ignored when two DAIs are being compared over the same anisotropy interval.

Standard propagation-of-error theory predicts that if one variable can be expressed in terms of another variable, for example FA(sRA) (Eq. [1]) and sRA(FA) (Eq. [4]), then the relative standard deviations are related (8) by

$$\sigma_{\mathrm{FA}}/\sigma_{\mathrm{sRA}} = d\mathrm{FA}/d\mathrm{sRA}. \quad [16]$$

Equation [16] applies to Eqs. [8–11] and is valid whether the scatter in the data is caused by noise or by biologic heterogeneity. Since dFA/dsRA equals the relative contrast between FA and sRA for small anisotropy differences, such pairs of variables should have identical CNR for small anisotropy differences. Therefore sRA, FA, $\mathrm{UA}_{\mathrm{surf}}$, and GV should have identical CNR, and VR and $\mathrm{UA}_{\mathrm{vol}}$ should have identical CNR. However, these equalities do not appear to have been published. Furthermore, it is not clear whether the CNR values of these two groups are equal and how they compare to the CNR of $\mathrm{UA}_{\mathrm{vol,\ surf}}$.

When two CNRs such as $\mathrm{CNR}_{\mathrm{FA}}$ and $\mathrm{CNR}_{\mathrm{sRA}}$ are being compared, application of Eq. [13] to each index yields

$$\frac{\mathrm{CNR}_{\mathrm{FA}}}{\mathrm{CNR}_{\mathrm{sRA}}} = \frac{\mathrm{FA}_2 - \mathrm{FA}_1}{\sqrt{(\sigma_{\mathrm{FA1}}^2 + \sigma_{\mathrm{FA2}}^2)}} \frac{\sqrt{(\sigma_{\mathrm{sRA1}}^2 + \sigma_{\mathrm{sRA2}}^2)}}{\mathrm{sRA}_2 - \mathrm{sRA}_1}, \quad [17]$$

which can be rearranged with Eq. [16], after dividing numerator and denominator by σ_{sRA1}, to

$$\frac{\mathrm{CNR}_{\mathrm{FA}}}{\mathrm{CNR}_{\mathrm{sRA}}} = \frac{\mathrm{FA}_2 - \mathrm{FA}_1}{\left(\frac{d\mathrm{FA}_1}{d\mathrm{sRA}_1}\right)\sqrt{\left[1 + \left(\frac{\sigma_{\mathrm{sRA2}}}{\sigma_{\mathrm{sRA1}}}\right)^2 \frac{\left(\frac{d\mathrm{FA}_2}{d\mathrm{sRA}_2}\right)^2}{\left(\frac{d\mathrm{FA}_1}{d\mathrm{sRA}_1}\right)^2}\right]}} \times \frac{\sqrt{\left[1 + \left(\frac{\sigma_{\mathrm{sRA2}}}{\sigma_{\mathrm{sRA1}}}\right)^2\right]}}{\mathrm{sRA}_2 - \mathrm{sRA}_1}. \quad [18]$$

Similar equations can be written for the other DAI pairs in Eqs. [8–11]. Equation [18] shows that the ratio $\mathrm{CNR}_{\mathrm{FA}}/\mathrm{CNR}_{\mathrm{sRA}}$ depends on only three parameters—the two sRA values and the ratio of the SDs at these two sRA values, $\sigma_{\mathrm{sRA2}}/\sigma_{\mathrm{sRA1}}$—because each sRA value determines the corresponding FA (Eq. [1]) and dFA/dsRA (Eq. [8]). When the two points approach a single value (a very small anisotropy interval), $\mathrm{CNR}_{\mathrm{FA}}/\mathrm{CNR}_{\mathrm{sRA}}$ approaches a value of 1. In general, the ratio $\mathrm{CNR}_{\mathrm{FA}}/\mathrm{CNR}_{\mathrm{sRA}}$ may be greater than 1 or less than 1, depending on the anisotropy interval and the variance in the data at each point.

Once the two anisotropy levels have been chosen, $\mathrm{CNR}_{\mathrm{FA}}/\mathrm{CNR}_{\mathrm{sRA}}$ increases when $\sigma_{\mathrm{sRA2}}/\sigma_{\mathrm{sRA1}}$ increases, and $\mathrm{CNR}_{\mathrm{FA}}/\mathrm{CNR}_{\mathrm{sRA}}$ decreases when $\sigma_{\mathrm{sRA2}}/\sigma_{\mathrm{sRA1}}$ decreases. A similar analysis could be performed for each other DAI pair in Eqs. [8–11]. In general, if the variance is greater where one DAI has a lower slope, then that DAI will have a more favorable CNR.

METHODS

Analytic Calculations

Analytic calculations were performed with standard propagation-of-error formulas (14). In one calculation, diffusion was measured along each of the three eigenvectors with $bD_{\mathrm{av}} = 0.5$, 1, or 1.5, where b is the diffusion sensitivity factor. Thus, each eigenvalue was measured directly in a single measurement. The propagation of error into each DAI was calculated by applying the formulas in Table 1 to these three eigenvalues. The CNR_1 for each DAI was then calculated over the range $A = 0$ to $A = 1$. In a second calculation the ratio $\mathrm{CNR}_{\mathrm{FA}}/\mathrm{CNR}_{\mathrm{sRA}}$ was calculated from Eq. [17] for two fixed anisotropy levels ($A = 0.1$ and 0.5) and several different values of the ratio $\sigma_{\mathrm{sRA2}}/\sigma_{\mathrm{sRA1}}$.

Simulations

Monte Carlo simulations, performed with IDL (Interactive Data Language, version 5.2, Research Systems, Inc., Boulder, CO), used six gradient pairs [(x, y), (x, $-y$), (y, z), (y, $-z$), (z, x), (z, $-x$)] with $bD_{\mathrm{av}} = 0.5$, 1, or 1.5. The starting point for each simulation was a cylindrically symmetric diffusion ellipsoid with its largest principal axis either along the z axis or rotated by $\pi/4$ radians about the x axis so that the largest principal axis was measured directly in the (y, $-z$) measurement. Gaussian-distributed noise (mean = 0 and | SD | = [$b = 0$ signal]/SNR) was added to each quadrature component of the $b = 0$ and diffusion-weighted signal intensities. The **D** matrix was calculated from the magnitudes of these seven noisy signals, and the DAIs were calculated from the eigenvalues (Table 1). The CNR_2 was calculated from Eq. [13] with A differences of 0.05 for 40000 trials with SNR = 25, 50, 100, and 1000 for the $b = 0$ signals.

For high A values or low SNR, the eigenvalue distribution had negative contributions. Although sRA and FA could still be between 0 and 1 with negative eigenvalues, VF would become greater than 1, creating an artifactually large variance. Therefore, the A range was restricted so that less than 0.3% of the eigenvalue distribution was negative, and negative eigenvalues were set to zero for the DAI calculations. This limited the simulations with $bD =$

1 to $A = 0$ to 0.50 for SNR = 25, $A = 0$ to 0.75 for SNR = 50, $A = 0$ to 0.85 for SNR = 100, and $A = 0$ to 0.95 for SNR = 1000 for the original ellipsoid. For the rotated ellipsoid, the ranges decreased further to $A = 0$ to 0.45 for SNR = 25 and $A = 0$ to 0.65 for SNR = 50. The resulting DAIs were not significantly affected by this small number of negative eigenvalues.

For comparison with published data (10), another set of simulations was performed with the parameters from that study. These simulations used the same six diffusion directions as above and a diagonal tensor with b = 1221 s/mm^2. The eigenvalues were 1700, 300, and 100 μm^2/s for the anisotropic tissue ($bD_{av} = 0.855$), modeled on the splenium, and 800 μm^2/s for isotropic diffusion ($bD_{av} = 0.977$). The anisotropic tissue was also compared to low levels of anisotropy with cylindrical symmetry ($A = 0.1$) and $D_{av} = 800$ μm^2/s. The expectation values and SDs of FA and sRA were calculated for 10000 repetitions with SNR = 20 and 100. In addition, the expectation values and SDs of FA and sRA with $bD_{av} = 1.0$ and cylindrical symmetry were calculated for $A = 0$ to 0.20 in steps of 0.01 with SNR = 20, 50, 100, 1000, and 10000. Negative eigenvalues were permitted for these simulations since only sRA and FA were being calculated.

Experimental Data

Measurements in the brain of a normal adult volunteer who gave informed consent were made under a protocol approved by our institutional review board. Diffusion-weighted images were acquired with a single-shot echo-planar imaging method, a field of view of 24 cm, 5-mm slice thickness, TE = 105 ms, TR = 6000 ms, b = 860 s/mm^2, and a 128 × 128 matrix. The gradient directions were the same as in the simulations, and each direction was repeated four times, two of which used the negative of the original gradient values. Signal intensities of the two images in each positive or negative direction were averaged, and then the geometric mean of each averaged direction and its negative direction was calculated to eliminate cross-terms between diffusion and imaging gradients (15). Four images with $b = 0$ were also acquired. The seven DAIs were calculated for each pixel to produce seven DAI maps. Each of 12 regions of interest (ROIs) was drawn on a DAI map that allowed clear visualization of the desired tissue as follows: thalamus, frontal white matter, internal capsule, genu, and splenium on FA maps; cortical gray matter, cerebral spinal fluid, putamen, centrum semiovale, and body of the corpus callosum on sRA maps; pons on a GV map; and brain stem on a UA_{vol} map. Each ROI avoided any areas where the eigenvalues were not calculated. For each ROI the means and SDs of all seven DAIs were calculated. Six ROIs with 46–86 pixels were selected for CSR calculation because of the moderate anisotropy differences between regions. In order of increasing anisotropy these were cortical gray matter, thalamus, centrum semiovale, pons, internal capsule, and splenium of the corpus callosum. The CSR for each DAI was calculated from Eq. [15] for the five pairs of ROIs with adjacent anisotropy values and for each tissue relative to gray matter and centrum semiovale. The SNR of the $b = 0$ images was calculated by measuring the background noise and correcting for the Rayleigh distribution (16,17).

RESULTS

Analytic Calculations

Analytic propagation-of-error calculations were made for each DAI in a simplified system where the three eigenvalues were measured in three independent measurements. The seven CNR_1 curves were identical over the entire anisotropy range. When bD_{av} was changed from 1 to 0.5 or 1.5, the shape of the curve changed, but in each case CNR_1 was identical for all seven DAIs over the entire anisotropy range.

In order to investigate larger anisotropy differences between two tissues, the CNR ratio for any DAI pair shown in Eqs. [1–7] is given by an equation similar to Eq. [18]. If $sRA_1 = 0.1$ and $sRA_2 = 0.5$, then as $\sigma_{sRA2}/\sigma_{sRA1}$ increases from 0.5 to 1.0 and 2.0, and CNR_{FA}/CNR_{sRA} increases from 0.86 to 0.98 and 1.19. This demonstrates that if noise increases at the higher anisotropy level, where the FA curve is flatter (Fig. 1), then FA will have an improved CNR relative to sRA.

Simulations with Small Anisotropy Differences

The CNR_2 calculated in simulations with $bD_{av} = 1$ and SNR = 50 is shown for each DAI as a function of A in Fig. 2. Curves for FA, GV, and UA_{surf} are not shown because they were almost identical to sRA. With the largest diffusion axis along the z axis, the curves were very similar for nearly isotropic diffusion, and the differences became more pronounced as A increased (Fig. 2a). When the ellipsoid was rotated by $\pi/4$ radians about the x axis, CNR at higher anisotropy levels decreased and the differences between groups were smaller (Fig. 2b). Calculation of CNR_2 for sRA at intermediate rotations in steps of $\pi/40$ radians revealed that the sRA curve became horizontal with a $3\pi/40$ radian rotation, and analytic calculations produced similar results. When random orientations were used, the results fell between the two extremes, with a slight negative slope (data not shown). At a lower SNR of 25, the curves diverged sooner and the differences between groups were greater, while at SNR = 100 or 1000 the curves diverged later and differences between groups were smaller (data not shown).

In each case the DAIs were easily divided into three groups based on CNR. The curves for Group 1 (sRA, FA, GV, and UA_{surf}) were virtually indistinguishable from each other, as expected from the algebraic relationships between these DAIs (Eqs. [1–4]). Similarly, Group 2 (VF and UA_{vol}) had similar CNR, as expected from the algebraic relationship of Eqs. [5] and [6], and this CNR was slightly lower than that of the first group. The lowest CNR occurred for $UA_{vol, surf}$. When the bD_{av} value was changed to 0.5 or 1.5, the shapes of the curves changed, but the same three groups were clearly seen, with similar differences between groups.

Simulations with Large Anisotropy Differences

Simulations were performed to calculate the ratio CNR_{FA}/CNR_{sRA} for the difference between a tissue with the diffusion properties of the splenium and a tissue with isotropic or nearly isotropic diffusion, similar to a published report (10). This ratio was slightly greater than 1 for isotropic

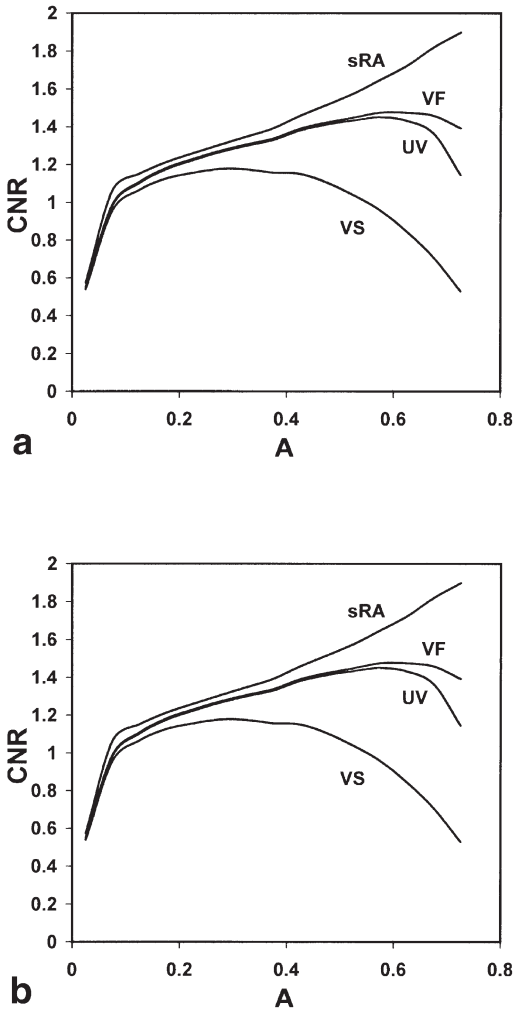

FIG. 2. CNR_2 as a function of A for four of the seven DAIs calculated in simulations with $bD_{av} = 1$. The diffusion ellipsoid is aligned with the reference frame (diagonal tensor) in **a** and rotated by $\pi/4$ radians about the x axis in **b**. Forty thousand repetitions were performed for $\Delta A = 0.05$ and SNR = 50. The curves for FA, GV, and UA_{surf} are not shown because they are almost identical to sRA. In **b**, the VF curve (not labeled) is nearly identical to the sRA curve at high anisotropy and just above the UV curve at low anisotropy. Abbreviations are the same as in Fig. 1.

diffusion, 1.06 with SNR = 100 and 1.05 with SNR = 20. However, with A = sRA = 0.1 the ratio decreased to 0.85 with SNR = 100 and 0.95 with SNR = 20. Thus, the apparent advantage of FA is not sustained if the conditions are changed slightly.

The apparent CNR advantage of FA for isotropic diffusion could be explained by an artifactually low variance for isotropic or nearly isotropic diffusion (17). To investigate this possibility, the SD of sRA was calculated in simulations with cylindrical symmetry over the range A = 0 to 0.20 for $bD_{av} = 1$ and several SNR levels (Fig. 3a). The calculated SDs were multiplied by SNR so that they could be compared directly. The curves for SNR = 1000 and 10000 are nearly identical, indicating minimal bias for $A >$ 0.01 at these SNR levels. In contrast, as SNR decreased from 1000 to 100, 50, and 20, the scaled SD of sRA decreased, especially at lower anisotropy levels, and approached the true values as anisotropy increased. This deviation of the SD from the true values parallels the positive bias in the calculated sRA values under the same conditions (Fig. 3b) (17).

Experimental Data

One $b = 0$ image and the corresponding FA and sRA maps are shown in Fig. 4. The ROIs for thalamus, internal capsule, and splenium were drawn on the FA map in Fig. 4b, avoiding the regions where no FA was calculated in the splenium, and the putamen ROI was drawn on the sRA map in Fig. 4c. The SNR of the $b = 0$ human brain images was estimated from the average signal intensity above the ventricles (485) and from background noise, which had a mean value of 24.1 and a SD of 17.2. After correction for

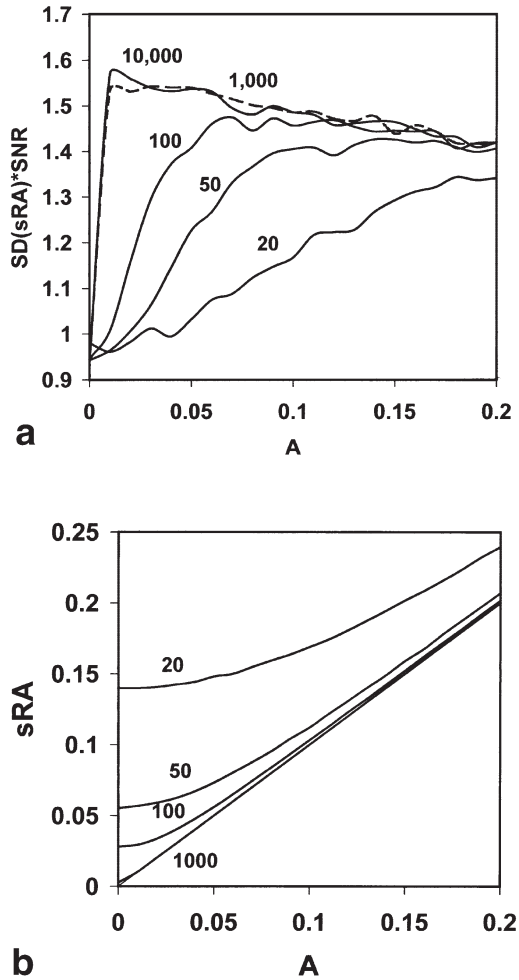

FIG. 3. **a**: SD of sRA at low anisotropy levels with SNR = 10000, 1000, 100, 50, and 20 from top to bottom. Standard deviations were calculated from simulations with cylindrical symmetry and $bD_{av} = 1$. Each SD has been multiplied by the SNR so that they can be compared directly on the same scale. **b**: Bias of sRA at low anisotropy levels with SNR = 1000, 100, 50, and 20 from bottom to top. The sRA value for A = 0 to 0.20 was calculated from simulations with cylindrical symmetry and $bD_{av} = 1$. The true value is indicated by a straight line that is mostly obscured by the SNR = 1000 line.

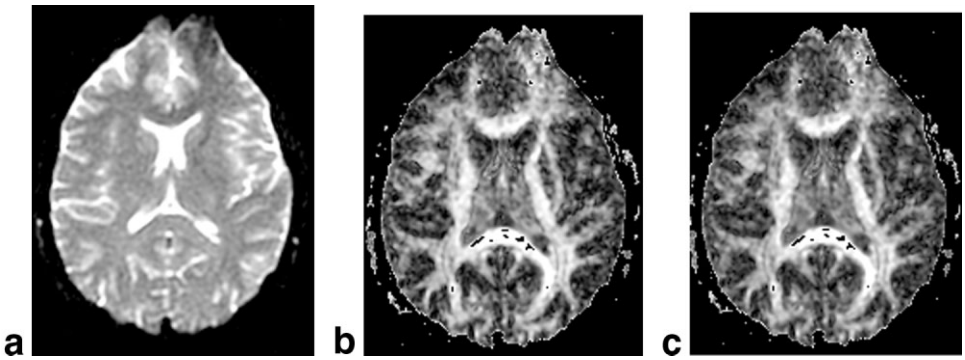

FIG. 4. (**a**) One $b = 0$ image of a human brain, (**b**) the FA map from the same slice, and (**c**) the sRA map from the same slice.

the Rayleigh distribution (16,17), the estimated noise level is $24.1/(\pi/2)^{1/2} = 19.2$ or $17.2/(2 - \pi/2)^{1/2} = 26.3$, yielding SNR = 25.3 or 18.4. When four acquisitions are averaged together, the expected SNR is between 36 and 50.

The calculated mean DAI values and standard deviations for six regions of interest in a human brain are shown in Table 2. The five CSR values calculated from Eq. [15], and the changes as a function of anisotropy, were similar for all seven DAIs (Fig. 5). The deviation of each DAI from the mean CSR of all seven DAIs was calculated. Six DAIs were within about 1 SD of the mean, while FA was 1.5 standard deviations above the mean. Thus, no DAI had a CSR that was significantly different from the mean value.

To investigate the possibility that the six selected ROIs had unusual variances, the mean and SD in all 12 ROIs with at least 33 pixels each were fitted with a polynomial curve for each DAI. The resulting CNR_1 plot, calculated from Eq. [14], was similar to Fig. 5.

Although CNR with small anisotropy differences is most important for comparing groups or regions with small anisotropy differences, larger anisotropy differences can also be considered. When gray matter was compared to the other five brain regions, the calculated CSR_{DAI}/CSR_{sRA} generally increased as the anisotropy increased for FA and GV, while it decreased for all three UA indices (Table 3). When the centrum semiovale was used as a reference, the patterns changed considerably (Table 4).

DISCUSSION

The results of diffusion-weighted imaging and DTI measurements can be predicted by analytic propagation-of-error calculations (3,8,18–20) and by Monte Carlo simulations (2,4–6,9–11,21,22). The propagation-of-error approach is useful for measuring a single apparent diffusion coefficient (ADC) (18,19), for measuring the three diffusion eigenvalues in three separate and independent measurements (3,20), and for limited segments of the DTI data processing chain, as in Eq. [16] (8). This approach may work for the entire DTI processing chain with six diffusion directions, but those analytic formulas would be very complex and have not been published.

The propagation-of-error approach for the entire DTI processing chain fails when diffusion is measured in more than six directions because the error in each diffusion measurement propagates into all six tensor elements in complex ways. Furthermore, error propagation has two other limitations. First, it assumes a first-order linear approximation of the function. This approximation begins to break down as SNR decreases and as anisotropy increases (Fig. 2b). Second, error propagation does not predict the bias in DAI values (Fig. 3b) (5,6,11) and SDs (Fig. 3a). Although the SD bias does not appear to have been reported previously, it is visible in Fig. 4e of Ref. (5) where the SD curves for sRA and FA, which increase as λ_1/λ_3 decreases from 10 ($A = 0.75$) to 2 ($A = 0.25$), level off (FA) or decline (sRA) between $\lambda_1/\lambda_3 = 2$ and $\lambda_1/\lambda_3 = 1$ ($A = 0$). Therefore, simulations are used for more realistic predictions of DTI measurements, even with six measurement directions.

The propagation-of-error formula in Eq. [16] predicts that the DAI pairs in Eqs. [8–11] should have identical CNR_1. In fact, the theoretical CNR_1 is identical for all seven DAIs. This same theory predicts that as nonlinear effects increase with lower SNR and increased anisotropy, differences will appear between groups before they appear within a group. The simulations shown in Fig. 2 support these predictions. The orientation dependence of the CNR seen in Fig. 2 would nearly disappear if the number of diffusion directions were increased from 6 to 15–21 (21).

Table 2
Comparison of DAIs between Different Brain Regions[a]

ROI	sRA	FA	GV	UA_{surf}	VF	UA_{vol}	$UA_{vol,surf}$
Gray matter	0.048 (0.015)	0.083 (0.027)	0.0088 (.0071)	0.0012 (0.0008)	0.0076 (0.0048)	0.0025 (0.0016)	0.0012 (0.0008)
Thalamus	0.158 (0.018)	0.266 (0.029)	0.138 (0.032)	0.013 (0.0028)	0.077 (0.015)	0.026 (0.0051)	0.014 (0.0025)
Centrum semiovale	0.261 (0.033)	0.424 (0.047)	0.353 (0.071)	0.035 (0.0091)	0.183 (0.042)	0.066 (0.016)	0.031 (0.0083)
Pons	0.470 (0.064)	0.674 (0.061)	0.724 (0.079)	0.120 (0.038)	0.489 (0.100)	0.205 (0.058)	0.097 (0.031)
Internal capsule	0.562 (0.062)	0.759 (0.049)	0.830 (0.053)	0.176 (0.045)	0.647 (0.086)	0.298 (0.062)	0.149 (0.036)
Splenium	0.703 (0.063)	0.861 (0.039)	0.927 (0.030)	0.294 (0.065)	0.818 (0.085)	0.450 (0.097)	0.226 (0.077)

[a]Values are the mean of 46–86 pixels. Standard deviations are shown in parentheses.

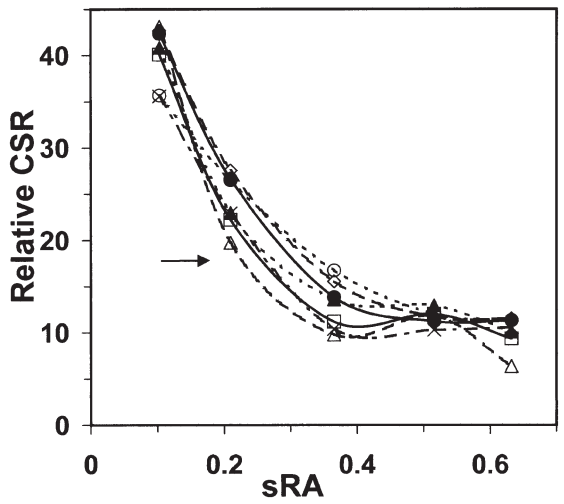

FIG. 5. CSR between six regions of the human brain as a function of sRA for the seven DAIs. The sRA shown for each CSR is the average of the two regions. The curves from left to right at the arrow are $UA_{vol,\ surf}$ (Δ), UA_{vol} (□), UA_{surf} (X), VF (▲), sRA (●), FA (◇), and GV (○).

Because CNR is a statistically meaningful measurement, CNR equivalence means that FA and RA have equal ability to differentiate tissues with different anisotropies. DAI comparisons based on "sensitivity" defined as the derivative with respect to A (4,7), or "noise immunity" defined as the calculated SNR (8), do not provide any useful information on the statistical advantage of one DAI over another. For example, FA as a function of A is concave down, sRA is linear, GV is sigmoid, and UA_{surf} is concave up (Fig. 1). However, for small anisotropy differences, all four indices have identical theoretical CNR_1, and very similar CNR_2 (Fig. 2) and CSR (Fig. 5), over the entire anisotropy range. For large anisotropy differences, small CNR differences may be calculated in specific instances, but no consistent advantage of any of the four DAIs over any other one is found. Therefore, these four DAIs are equally good for determining whether anisotropy is the same or different in two homogeneous regions.

All seven DAIs had similar CSR for small anisotropy differences in human brain (Fig. 5). The scatter in the brain data were apparently large enough to mask any small differences expected between the DAIs. The experimental CSR decline with anisotropy (Fig. 5) appears to be real, because a plot of published data (2) yields a shape similar to Fig. 5 with an approximate threefold CSR decrease. Since the CSR decline in Fig. 5 occurs at a lower anisotropy level than predicted by even the lowest CNR simulations (Fig. 2b), it cannot be explained completely by noise and must be caused partly by heterogeneity within each tissue.

When tissues with very different anisotropies are considered, analysis of published FA and sRA data (2) yields results similar to Tables 3 and 4. The contrast is proportional to the average slope of a DAI between two A values, while the relative SD depends on the slopes at the A values (Eq. [16]). Thus, an appropriate sigmoid curve will provide the highest CSR between two very different tissues, for example, GV in Tables 3 and 4. However, this may not provide the best CSR between other pairs of tissues (Tables 3 and 4).

Equation [16] predicts that when two tissues with very different anisotropy levels are compared, if the SD increases significantly with anisotropy, then CSR_{FA} will increase relative to CSR_{sRA}. Table 2 shows that the measured SD generally increases with anisotropy in human brain, similar to published results (2). Therefore, the calculated CSR between tissues with large anisotropy differences is greater for FA than for sRA (Table 3). The increased SD with increasing anisotropy appears to have three contributing factors. First, at very low anisotropy levels there is a negative SD bias (Fig. 3a). Second, as anisotropy increases, the range of ADCs being measured increases, requiring that some ADCs be further from their optimum b factor. Third, anisotropic tissues appear to have more biologic heterogeneity, as suggested by the sharp decline in CSR at moderate anisotropy levels (Fig. 5).

It has been suggested that the DAIs with the lowest values for an isotropic phantom are less sensitive to noise when anisotropy is low (4). However, our results show that all seven DAIs have virtually identical CNR when anisotropy is low, and thus all would be equally good for distinguishing slightly anisotropic diffusion from isotropic diffusion (Fig. 2).

CONCLUSIONS

All seven proposed rotationally invariant DAIs that do not require eigenvalue sorting have similar CNR for small anisotropy differences under a wide range of conditions. Calculated CNR, especially for larger anisotropy differences, may be affected by the bias in the DAI values and in their SDs, by the choice of b factor, and by nonuniform diffusion anisotropy within a region of interest. Small CNR

Table 3
Comparison of CSR_{DAI}/CSR_{sRA} between Gray Matter and Tissues with Different Anisotropies

Tissue	Anisotropy index					
	FA	GV	UA_{surf}	VF	UA_{vol}	$UA_{vol,surf}$
Thalamus	1.01	0.84	0.84	0.96	0.95	1.02
Centrum semiovale	1.08	0.82	0.64	0.70	0.66	0.62
Pons	1.39	1.41	0.49	0.76	0.55	0.48
Internal capsule	1.49	1.90	0.48	0.92	0.59	0.51
Splenium	1.64	3.00	0.45	0.95	0.46	0.29

Table 4
Comparison of CSR_{DAI}/CSR_{sRA} between Centrum Semiovale and Tissues with Different Anisotropies

Tissue	Anisotropy index					
	FA	GV	UA_{surf}	VF	UA_{vol}	$UA_{vol,surf}$
Gray matter	1.08	0.82	0.64	0.70	0.66	0.62
Thalamus	1.03	0.99	0.86	0.86	0.83	0.74
Pons	1.12	1.21	0.75	0.98	0.81	0.71
Internal capsule	1.15	1.25	0.71	1.12	0.85	0.74
Splenium	1.16	1.20	0.63	1.08	0.63	0.40

differences appear in certain circumstances, including low SNR and high anisotropy levels. However, FA does not have any intrinsic advantage over sRA.

REFERENCES

1. Le Bihan D, Mangin JF, Poupon C, Clark CA, Pappata S, Molko N, Chabriat H. Diffusion tensor imaging: concepts and applications. J Magn Reson Imaging 2001;13:534–546.
2. Alexander AL, Hasan K, Kindlmann G, Parker DL, Tsuruda JS. A geometric analysis of diffusion tensor measurements of the human brain. Magn Reson Med 2000;44:283–291.
3. Papadakis NG, Xing D, Houston GC, Smith JM, Smith MI, James MF, Parsons AA, Huang CLH, Hall LD, Carpenter TA. A study of rotationally invariant and symmetric indices of diffusion anisotropy. Magn Reson Imaging 1999;17:881–892.
4. Armitage PA, Bastin ME. Selecting an appropriate anisotropy index for displaying diffusion tensor imaging data with improved contrast and sensitivity. Magn Reson Med 2000;44:117–121.
5. Skare S, Li T, Nordell B, Ingvar M. Noise considerations in the determination of diffusion tensor anisotropy. Magn Reson Imaging 2000;18:659–669.
6. Pierpaoli C, Basser PJ. Toward a quantitative assessment of diffusion anisotropy. Magn Reson Med 1996;36:893–906. [Published erratum: Magn Reson Med 1997;37:972.]
7. Ulug AM, van Zijl PCM. Orientation-independent diffusion imaging without tensor diagonalization: anisotropy definitions based on physical attributes of the diffusion ellipsoid. J Magn Reson Imaging 1999;9:804–813.
8. Hasan KM, Alexander AL, Narayana PA. Does fractional anisotropy have better noise immunity characteristics than relative anisotropy in diffusion tensor MRI? An analytical approach. Magn Reson Med 2004;51:413–417.
9. Hasan KM, Narayana PA. Computation of the fractional anisotropy and mean diffusivity maps without tensor decoding and diagonalization: theoretical analysis and validation. Magn Reson Med 2003;50:589–598.
10. Sorensen AG, Wu O, Copen WA, Davis TL, Gonzalez RG, Koroshetz WJ, Reese TG, Rosen BR, Wedeen VJ, Weisskoff RM. Human acute cerebral ischemia: detection of changes in water diffusion anisotropy by using MR imaging. Radiology 1999;212:785–792.
11. Bastin ME, Armitage PA, Marshall I. A theoretical study of the effect of experimental noise on the measurement of anisotropy in diffusion imaging. Magn Reson Imaging 1998;16:773–785.
12. Conturo TE, McKinstry RC, Akbudak E, Robinson BH. Encoding of anisotropic diffusion with tetrahedral gradients: a general mathematical diffusion formalism and experimental results. Magn Reson Med 1996;35:399–412.
13. Basser PJ. Inferring microstructural features and the physiological state of tissues from diffusion-weighted images. NMR Biomed 1995;8:333–344.
14. Bevington PR. Data reduction and error analysis for the physical sciences. New York: McGraw-Hill; 1969. 336 p.
15. Neeman M, Freyer JP, Sillerud LO. A simple method for obtaining cross-term-free images for diffusion anisotropy studies in NMR microimaging. Magn Reson Med 1991;21:138–143.
16. Gudbjartsson H, Patz S. The Rician distribution of noisy MRI data. Magn Reson Med 1995;34:910–914. [Letter, related letter, and response: Magn Reson Med 1996;36:331–333]
17. Edelstein WA, Glover GH, Hardy CJ, Redington RW. The intrinsic signal-to-noise ratio in NMR imaging. Magn Reson Med 1986;3:604–618.
18. Xing D, Papadakis NG, Huang CLH, Lee VM, Carpenter TA, Hall LD. Optimised diffusion-weighting for measurement of apparent diffusion coefficient (ADC) in human brain. Magn Reson Imaging 1997;15:771–784.
19. Jones DK, Horsfield MA, Simmons A. Optimal strategies for measuring diffusion in anisotropic systems by magnetic resonance imaging. Magn Reson Med 1999;42:515–525.
20. Kingsley PB, Monahan WG. Selection of the optimum b factor for diffusion-weighted magnetic resonance imaging assessment of ischemic stroke. Magn Reson Med 2004;51:996–1001.
21. Papadakis NG, Murrills CD, Hall LD, Huang CL, Carpenter TA. Minimal gradient encoding for robust estimation of diffusion anisotropy. Magn Reson Imaging 2000;18:671–679.
22. Batchelor PG, Atkinson D, Hill DL, Calamante F, Connelly A. Anisotropic noise propagation in diffusion tensor MRI sampling schemes. Magn Reson Med 2003;49:1143–1151.